Synthesis of Highly Active Pt-Pd-Cu/C Catalysts for Formic Acid Oxidation

Yange Suo[*]*, Yuxin Guo, Chenbin Rong, Zhiguo Zhang, Guilin Hu*

Department of Energy and Environmental Systems Engineering, Zhejiang University of Science and Technology, Liuhe Road 318#, Hangzhou, Zhejiang Province 310023, China
[*]E-mail: suoyg@126.com

This work reports the synthesis of a series of carbon supported Pt-Pd-Cu (Pt-Pd-Cu/C) nano-catalysts for formic acid oxidation. The trimetallic catalysts were prepared by a one-pot protocol through reduction of Pt, Pd and Cu ions using ethylene glycol and sodium citrate as the reducing and stabilizing reagents. XRD characterization suggests that Pt-Pd-Cu alloys with different lattice parameters can be successfully prepared through adjusting the atomic ratios of Pt, Pd and Cu ions in the precursor solutions. The average crystal sizes of the Pt-Pd-Cu/C catalysts are in the range of 2.7-3.1 nm. TEM images shows that the metallic nanoparticles are well dispersed on the carbon surface, with $Pt_1Pd_3Cu_3/C$ catalyst showing obvious aggregation. XPS was carried out to analyze the surface compositions, as well as the chemical states of the novel metals in the catalysts. The real atomic ratios of the metals in the catalysts based on ICP-OES evaluation are consistent with the stoichiometric values. Electrochemical analysis suggests that the activities the Pt-Pd-Cu/C catalysts towards formic acid oxidation are dependent on the composition of the catalysts, with $Pt_1Pd_4Cu_2/C$ exhibiting the best performance. A mass normalized peak current density of 3.02 $A/mg_{(Pt+Pd)}$ was observed on $Pt_1Pd_4Cu_2/C$ catalyst.

1. INTRODUCTION

The exploration of new materials for formic acid oxidation reaction has received lots of attention in recent years due to the promising application of direct formic acid fuel cells. Pt and Pd have been widely studied as active materials for catalyzing formic acid oxidation [1, 2]. It is now widely accepted that formic acid oxidation follows a dual-path mechanism [3], i. e., a dehydrogenation pathway to form CO_2 directly via reactive intermediates and a dehydration pathway to generate

poisonous CO_{ads}, which could only be removed at high potential range. On Pt surface, the dehydration of formic acid oxidation is dominant and thus the activity of Pt is greatly affected [4]. Although Pd favors the dehydrogenation of formic acid to form CO_2 [5], the poor electrochemical stability of Pd greatly affects its practical applications [6]. Besides, both Pt and Pd are precious metals, resulting in the high cost of the catalysts for fuel cell. Therefore, development of less expensive and more active materials for formic acid oxidation is still highly demanding.

Alloying Pt or Pd with another metals is one of the most effective ways to reduce the loading of noble metals. Moreover, the electronic or geometric structure of Pt-based or Pd-based binary materials could be greatly different from the monometallic Pt or Pd, and thus enhanced activity of Pt-based or Pd-based binary catalysts have been obtained. For instance, PtCo [7], PtFe [8], PtBi [9], PtAg [10], PtSn [11], PtCu [12], PdIr [13], PdCo [14], PdNi [15], PdRh [16], PdAg [17], PdCr [18], PdCu [19], PdAu [20], PdPt [21] have been reported to exhibit better performance towards formic acid oxidation than single Pt or Pd. The enhanced activities are usually ascribed to the adjusted electronic effect [22], structural effect [23] or synergistic effect [24]. Besides binary catalysts, some efforts have also been put to explore ternary material due to the more flexibility of adjusting the electronic properties. For instance, Yu et al., [25] have prepared carbon supported ternary Pd-Cu-Fe catalyst with high performance for formic acid oxidation. Fu et al., [26] have synthesized trimetallic PtAgCu@PtCu core@shell concave nanooctahedrons through a one-pot hydrothermal reduction method. The as-prepared catalyst exhibit a superior electro-catalytic activity towards formic acid oxidation compared with commercial Pt black. Cui et al., [27] have studied the active site of PtPdCu catalyst for formic acid oxidation. The coverage of Pt atoms on the topmost surface layer has an influence on its activity. Jiang et al., [28] have synthesized Pd-Pt-Cu nanocatalysts through reduction by $NaBH_4$ with either disodium ethylenediamine tetraacetate (EDTA) as the stabilizer in aqueous solution or oleylamine (OAm) as the stabilizer in anhydrous ethanol, as well as using ethylene glycol as the reducing reagent and sodium citrate or urea as the stabilizing reagent. Electrochemical evaluation suggests that Pd-Pt-Cu nanocatalysts synthesized using ethylene glycol as the reducing reagent and sodium citrate as the stabilizing reagent exhibits the highest activity towards formic acid oxidation. They have also synthesized three Pd-Pt-Cu nanocatalysts containing trace amount of Pt (atomic content of Pt lower than 7%) and investigated the composition-dependent activity. However, they have not explored the activity of Pd-Pt-Cu with a relatively high content of Pt towards formic acid oxidation.

In this work, a series of carbon supported Pt-Pd-Cu trimetallic (Pt-Pd-Cu/C) nano-catalysts (metallic loading of 20 wt %, atomic ratios of Pt to Pd to Cu being 1:1:1, 1:2:1, 1:5:1, 1:4:2, 1:3:3) were prepared towards formic acid oxidation reaction. The trimetallic catalysts were prepared through simply co-reduction of Pt, Pd and Cu ions using ethylene glycol and sodium citrate as the reducing and stabilizing reagents. XRD, TEM, XPS, ICP-OES were carried out to characterize the physiochemical properties of the catalysts. Electrochemical analysis suggests that the mass activities of the Pt-Pd-Cu/C activities are dependent on the composition of the catalysts, with $Pt_1Pd_4Cu_2$/C exhibiting the highest value.

2. EXPERIMENTAL

2.1. Chemicals

Chloroplatinic acid hexahydrate ($H_2PtCl_6\cdot6H_2O$), copper (II) sulfate pentahydrate ($CuSO_4\cdot5H_2O$), ethylene glycol ($C_2H_6O_2$), perchloric acid ($HClO_4$), sodium citrate ($C_6H_5Na_3O_7\cdot2H_2O$), and ethanol (C_2H_5OH) were purchased from Sinopharm Chemical Reagent Co., Ltd. Ammonium tetrachloropalladate ((NH_4)$_2PdCl_4$) and formic acid (HCOOH) were ordered from Aladdin. Vulcan XC-72 carbon was purchased from E-TEK. Nafion solution (5 %) was received from Dupont. All chemicals were of analytical grade and used as received.

2.2. Synthesis of the catalysts

Carbon supported Pt-Pd-Cu catalysts with different compositions (metallic loading of 20 wt %, atomic ratios of Pt to Pd to Cu being 1:1:1, 1:2:1, 1:5:1, 1:4:2, 1:3:3) were prepared according to our previous report [29]. The synthesis of carbon supported Pt-Pd-Cu catalyst with atomic ratio of Pt to Pd to Cu of 1:1:1 was taken as an example to describe the detailed synthesis procedure. Firstly, 0.5793 g sodium citrate was dissolved into a solution containing 40 ml water and 40 ml ethylene glycol, and then 96 mg Vulcan XC-72 carbon was poured into the above solution which was stirred and ultrasonically mixed for 2 h to obtain the sodium citrate suspension. At the same time, 3.5 ml chloroplatinic acid hexahydrate ($H_2PtCl_6\cdot6H_2O$) aqueous solution (1 g / 100 ml), 23.32 mg ammonium tetrachloropalladate ((NH_4)$_2PdCl_4$) and 16.6 mg copper (II) sulfate pentahydrate ($CuSO_4\cdot5H_2O$) were dissolved into 15 ml water / ethylene glycol mixture solution (containing 7.5 ml water and 7.5 ml ethylene glycol) to obtain the precursor solution. After removing air with N_2 bubbling for 30 minutes, the sodium citrate suspension was refluxed at 170 ^{o}C oil bath for 15 minutes. Then, the precursor solution was added into the heated sodium citrate suspension drop by drop. Another 55 ml water / ethylene glycol solution (volume / volume = 1:1) was added into the reaction system, which was then continued to be heated for another 2 h. The reaction product was filtered and washed with water and ethanol. The residue was dried at 60 ^{o}C for 12 h and then grounded in an agate mortar to get the carbon supported Pt-Pd-Cu nanoparticles (denoted as $Pt_1Pd_1Cu_1$/C). Carbon supported Pt-Pd-Cu catalysts with atomic ratios of Pt to Pd to Cu of 1:2:1, 1:5:1, 1:4:2, 1:3:3 were denoted as $Pt_1Pd_2Cu_1$/C, $Pt_1Pd_5Cu_1$/C, $Pt_1Pd_4Cu_2$/C and $Pt_1Pd_3Cu_3$/C respectively. Carbon supported Pd nanoparticles (denoted as Pd/C) with Pd loading of 20 wt % and carbon supported Pt nanoparticles (denoted as Pt/C) with Pt loading of 20 wt % were also prepared using the same protocol for comparison.

2.3. Physicochemical characterization

Powder X-ray diffraction (XRD) was carried out with an X-ray diffractometer (Ultima IV, Rigaku) using a Cu Kα radiation source. The values of diffraction angle and breadth of diffraction line at half-maximum intensity, obtained through fitting of (220) diffraction peak to a Lorentzian line shape, were used to calculate the crystalline size and lattice parameter. Transmission electron

microscopy (TEM) was carried out with a JEM 2100 TEM system operated with LaB_6 filament at 200 kV. X-ray photoelectron spectroscopy (XPS) was carried out with a PHI500 system. Inductively coupled plasma-Optical Emission Spectrometer (ICP-OES) was carried out with a VISTAMPXICP-720 system.

2.4. Electrochemical evaluation

Electrochemical measurements were carried out using a CHI potentiostat (CHI600E). To do the electrochemical experiments, a conventional three-electrode cell, with a catalyst coated glassy carbon electrode (working electrode), a Pt coil (counter electrode) and a saturated Ag/AgCl electrode (reference electrode), was put into a 25 ^{o}C water tank. The glassy carbon substrate was polished with alumina suspension prior to use. To prepare the working electrode, 10 mg catalyst was dispersed ultrasonically in 2 ml diluted nafion solution (0.05 wt % in ethanol) for 30 minutes and 10 μl of the suspension was pipetted onto the glassy carbon electrode (d = 5 mm) by a microsyringe and left to dry at room temperature. Prior to the activity measurement, the working electrode was cleaned by cyclic voltammogram (CV) sweeping in N_2-saturated 0.5 M $HClO_4$ solution. Then, certain amount (in order to keep the concentration in the electrolyte as 0.5 M) of formic acid was added into the electrolyte to do the activity measurements. The currents in this manuscript were normalized by the total mass of Pt and Pd (analyzed by ICP-OES) on the glassy carbon electrode to give mass current densities, whose units are $A/mg_{(Pt+Pd)}$.

3. RESULTS AND DISCUSSION

3.1. Structure and morphology characterization
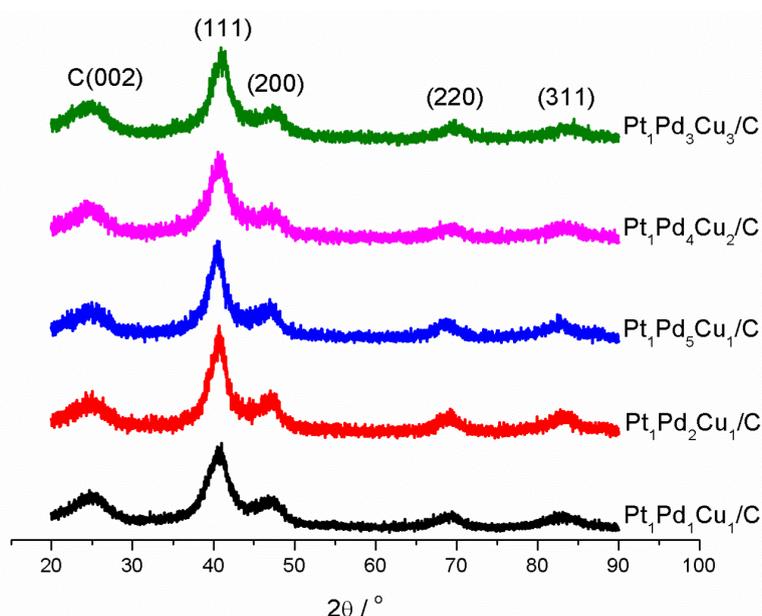
Figure 1. XRD patterns of the $Pt_1Pd_1Cu_1/C$, $Pt_1Pd_2Cu_1/C$, $Pt_1Pd_5Cu_1/C$, $Pt_1Pd_4Cu_2/C$, $Pt_1Pd_3Cu_3/C$ catalysts

Table 1. Crystalline sizes and lattice parameters of the Pt-Pd-Cu/C catalysts with different compositions based on XRD characterization

Sample	Crystalline size (nm)	Lattice parameter (Å)
$Pt_1Pd_1Cu_1$/C	2.7	3.848
$Pt_1Pd_2Cu_1$/C	3.1	3.847
$Pt_1Pd_5Cu_1$/C	3.1	3.863
$Pt_1Pd_4Cu_2$/C	3.0	3.842
$Pt_1Pd_3Cu_3$/C	2.8	3.820
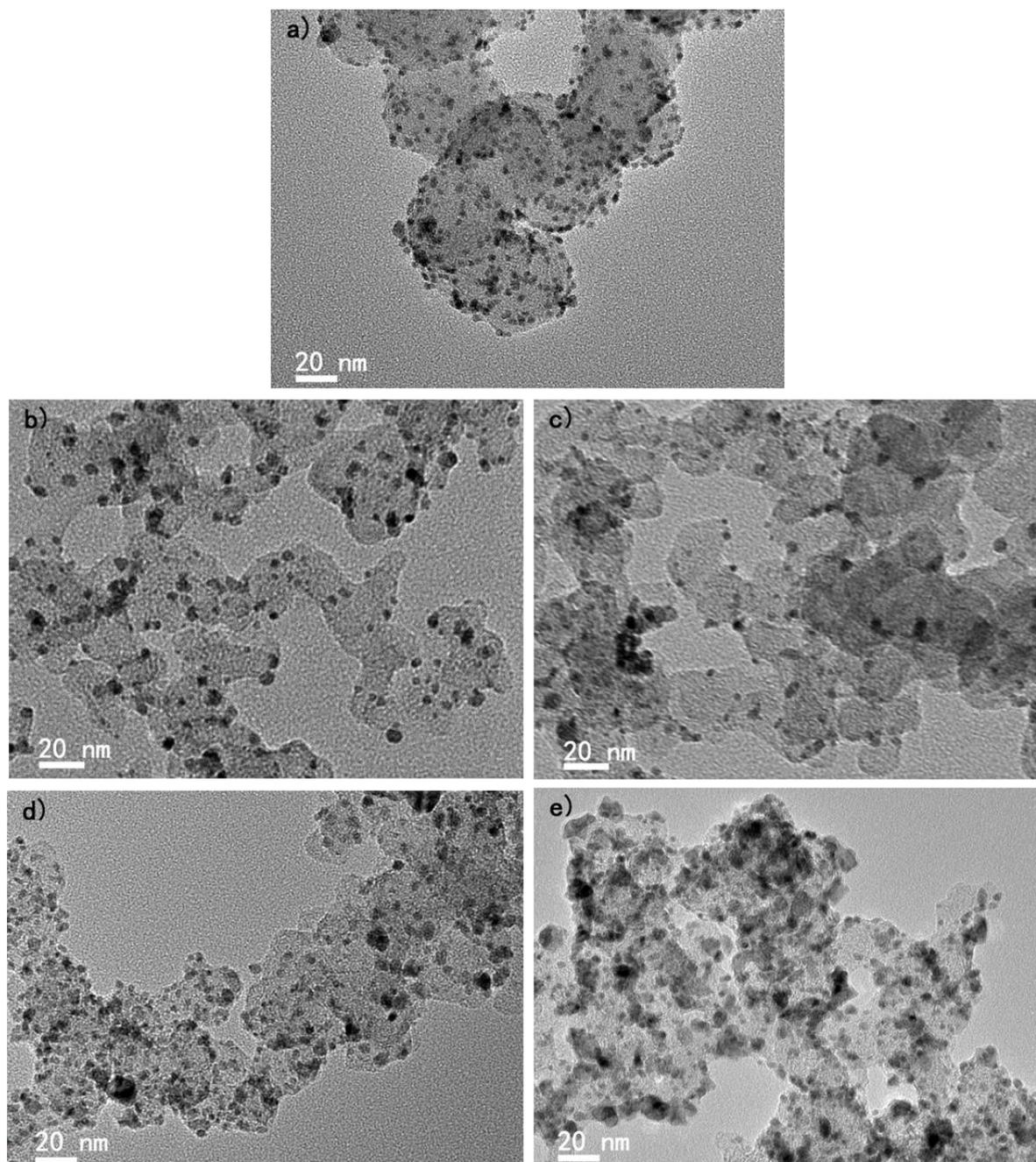
Figure 2. TEM images of the **a)** $Pt_1Pd_1Cu_1$/C; **b)** $Pt_1Pd_2Cu_1$/C; **c)** $Pt_1Pd_5Cu_1$/C; **d)** $Pt_1Pd_4Cu_2$/C; **e)** $Pt_1Pd_3Cu_3$/C catalysts
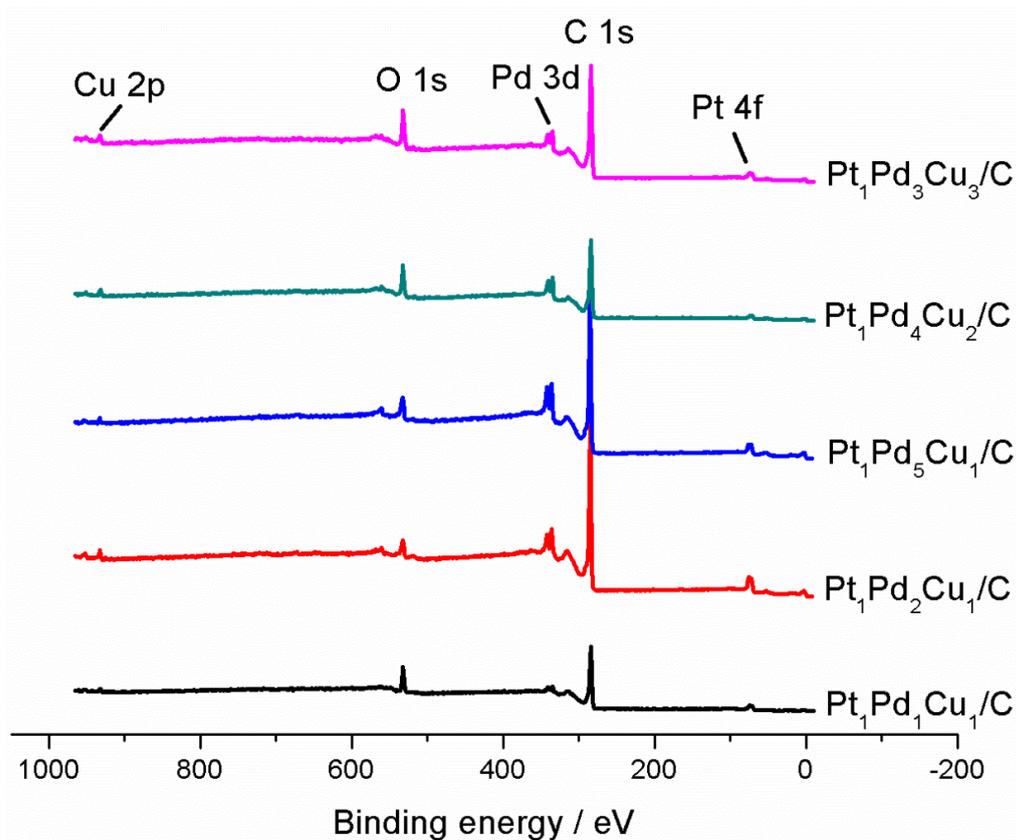
Figure 3. XPS spectra of the $Pt_1Pd_1Cu_1/C$, $Pt_1Pd_2Cu_1/C$, $Pt_1Pd_5Cu_1/C$, $Pt_1Pd_4Cu_2/C$, $Pt_1Pd_3Cu_3/C$ catalysts

XRD patterns of the $Pt_1Pd_1Cu_1/C$, $Pt_1Pd_2Cu_1/C$, $Pt_1Pd_5Cu_1/C$, $Pt_1Pd_4Cu_2/C$, $Pt_1Pd_3Cu_3/C$ catalysts are shown in Figure 1. The broad diffraction peak at about 25 ^{o} is assigned to the (002) plane of Vulcan XC-72 carbon. A single group of characteristic diffraction peaks of face centered cubic (fcc) crystalline structure can be observed on all the Pt-Pd-Cu/C catalysts. The lattice parameters of the catalysts calculated based on Bragg's law [30] using (220) diffraction peak are shown in Table 1. The lattice parameters of the Pt-Pd-Cu/C catalysts are smaller than that of the standard value of Pt (3.924 Å) or Pd (3.891 Å). Since the atomic radius of Cu is smaller than that of Pt or Pd, incorporation of Cu to the lattice of Pt or Pd could induce the lattice strain phenomena. Therefore, the reduced lattice parameters of the Pt-Pd-Cu/C catalysts could suggest the formation of alloy structure. From the data of $Pt_1Pd_5Cu_1/C$, $Pt_1Pd_4Cu_2/C$, $Pt_1Pd_3Cu_3/C$, it can be seen that when the content of Pt keeps unchanged, the lattice parameter of the trimetallic catalyst decreases with the increase of Cu content. The average crystalline sizes of the Pt-Pd-Cu/C are in the range of 2.7-3.1 nm.

TEM images of the $Pt_1Pd_1Cu_1/C$, $Pt_1Pd_2Cu_1/C$, $Pt_1Pd_5Cu_1/C$, $Pt_1Pd_4Cu_2/C$, $Pt_1Pd_3Cu_3/C$ catalysts are shown in Figure 2. It can be seen that, the nanoparticles in $Pt_1Pd_1Cu_1/C$, $Pt_1Pd_2Cu_1/C$ catalysts are well dispersed on the carbon surface. However, when the content of Pt is low, as in the $Pt_1Pd_5Cu_1/C$, $Pt_1Pd_4Cu_2/C$, $Pt_1Pd_3Cu_3/C$ catalyst, particle aggregation can be observed, with $Pt_1Pd_3Cu_3/C$ showing obvious aggregates.

Figure 3 shows the XPS spectra of the $Pt_1Pd_1Cu_1/C$, $Pt_1Pd_2Cu_1/C$, $Pt_1Pd_5Cu_1/C$, $Pt_1Pd_4Cu_2/C$, $Pt_1Pd_3Cu_3/C$ catalysts. Pt 4f, Pd 3d and Cu 2p spectra can be observed on all the catalysts. Figure 4 shows the Pt 4f high resolution spectra of all the Pt-Pd-Cu/C catalysts. A doublet including a low energy band (Pt $4f_{7/2}$) and a high energy band (Pt $4f_{5/2}$) can be observed. The chemical valance of Pt can be obtained through fitting the spectra to three pairs of overlapping curves, labeled as 1, 2, and 3, which can be ascribed to be Pt(0) chemical state, Pt(II) chemical state and Pt(IV) chemical state respectively [10]. The binding energies and relative intensities of the Pt 4f of the three catalysts are shown in Table 2. The relative intensities of Pt(0) in the $Pt_1Pd_1Cu_1/C$, $Pt_1Pd_2Cu_1/C$, $Pt_1Pd_5Cu_1/C$, $Pt_1Pd_4Cu_2/C$, $Pt_1Pd_3Cu_3/C$ catalysts are 37 %, 46 %, 42 %, 50 % and 39 % respectively. Figure 5 shows the regional Pd 3d spectra of all the Pt-Pd-Cu/C catalysts. Similar to Pt 4f, Pd 3d also shows a doublet containing a low energy band (Pd $3d_{5/2}$) and a high energy band (Pd $3d_{3/2}$). Two pairs of overlapping curves labeled as 1, and 2 can be ascribed to be Pd(0) chemical state and Pd(II) chemical state respectively. As shown in Table 3, the relative intensity of Pd(0) in the $Pt_1Pd_1Cu_1/C$, $Pt_1Pd_2Cu_1/C$, $Pt_1Pd_5Cu_1/C$, $Pt_1Pd_4Cu_2/C$, $Pt_1Pd_3Cu_3/C$ catalysts are 40 %, 42 %, 39 %, 54 % and 47 % respectively. Table 4 shows the surface metallic atomic ratios analyzed from XPS. It can be seen that the contents of Pd on the surface of the catalysts are consistent with the stoichiometric values. The contents of Pt are lower than their stoichiometric values, while the contents of Cu are higher than their stoichiometric values, indicating an enrichment of Cu on the surface.

Table 2. Binding energies, and relative intensities of different chemical states of Pt in the $Pt_1Pd_1Cu_1/C$, $Pt_1Pd_2Cu_1/C$, $Pt_1Pd_5Cu_1/C$, $Pt_1Pd_4Cu_2/C$, $Pt_1Pd_3Cu_3/C$ catalysts

Sample	Species	Binding energy (eV)	Relative intensity (%)
$Pt_1Pd_1Cu_1/C$	Pt(0)	71.6	37
	Pt(II)	72.6	52
	Pt(IV)	74.9	11
$Pt_1Pd_2Cu_1/C$	Pt(0)	71.6	46
	Pt(II)	72.4	33
	Pt(IV)	73.9	21
$Pt_1Pd_5Cu_1/C$	Pt(0)	71.5	42
	Pt(II)	72.4	32
	Pt(IV)	74.9	26
$Pt_1Pd_4Cu_2/C$	Pt(0)	71.5	50
	Pt(II)	72.6	21
	Pt(IV)	75.6	29
$Pt_1Pd_3Cu_3/C$	Pt(0)	71.5	39
	Pt(II)	72.4	22
	Pt(IV)	73.9	39
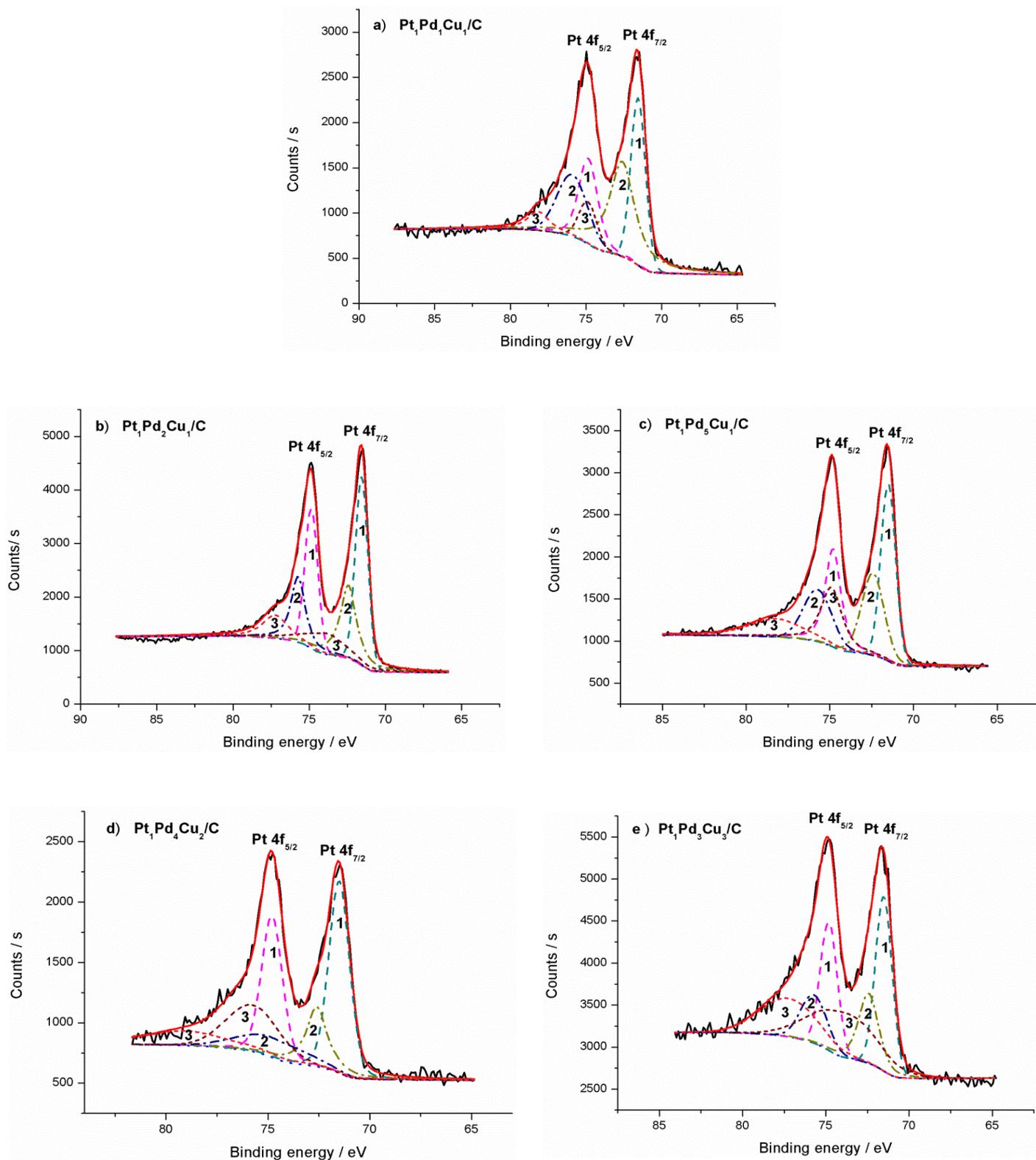
Figure 4. Pt 4f spectra of the $Pt_1Pd_1Cu_1/C$, $Pt_1Pd_2Cu_1/C$, $Pt_1Pd_5Cu_1/C$, $Pt_1Pd_4Cu_2/C$, $Pt_1Pd_3Cu_3/C$ catalysts

ICP-OES was carried out to determine the real metallic loadings of the catalysts. As shown in Table 5, the real atomic ratios of Pt to Pd to Cu in the Pt-Pd-Cu/C catalysts are consistent with the

stoichiometric values. Besides, the metallic loadings of the Pt-Pd-Cu/C are close to the stoichiometric value (i. e., 20 wt %).
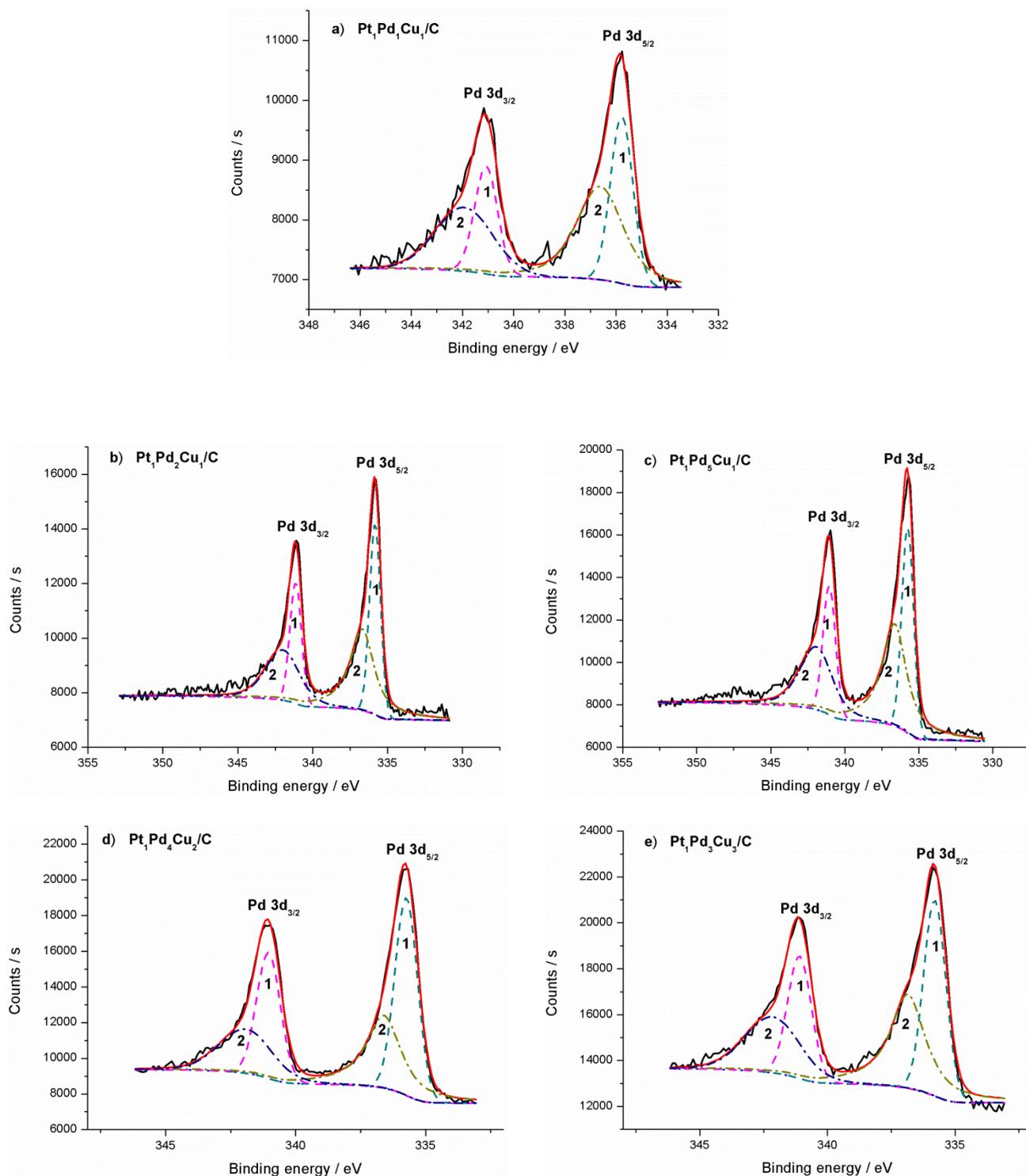
Figure 5. Pd 3d spectra of the $Pt_1Pd_1Cu_1$/C, $Pt_1Pd_2Cu_1$/C, $Pt_1Pd_5Cu_1$/C, $Pt_1Pd_4Cu_2$/C, $Pt_1Pd_3Cu_3$/C catalysts

Table 3. Binding energies, and relative intensities of different chemical states of Pd in the $Pt_1Pd_1Cu_1/C$, $Pt_1Pd_2Cu_1/C$, $Pt_1Pd_5Cu_1/C$, $Pt_1Pd_4Cu_2/C$, $Pt_1Pd_3Cu_3/C$ catalysts

Sample	Species	Binding energy (eV)	Relative intensity (%)
$Pt_1Pd_1Cu_1/C$	Pd(0)	335.8	40
	Pd(II)	337.6	60
$Pt_1Pd_2Cu_1/C$	Pd(0)	335.8	42
	Pd(II)	336.7	58
$Pt_1Pd_5Cu_1/C$	Pd(0)	335.8	39
	Pd(II)	336.6	61
$Pt_1Pd_4Cu_2/C$	Pd(0)	335.7	54
	Pd(II)	336.6	46
$Pt_1Pd_3Cu_3/C$	Pd(0)	335.8	47
	Pd(II)	336.9	53

Table 4. The stoichiometric, real atomic ratios analyzed from XPS in the $Pt_1Pd_1Cu_1/C$, $Pt_1Pd_2Cu_1/C$, $Pt_1Pd_5Cu_1/C$, $Pt_1Pd_4Cu_2/C$, $Pt_1Pd_3Cu_3/C$ catalysts

Sample	Stoichiometric atomic ratio of Pt to Pd to Cu	Atomic ratio of Pt to Pd to Cu from XPS
$Pt_1Pd_1Cu_1/C$	33: 33: 33	16: 35: 49
$Pt_1Pd_2Cu_1/C$	25: 50: 25	19: 52: 29
$Pt_1Pd_5Cu_1/C$	14: 72: 14	9: 65: 26
$Pt_1Pd_4Cu_2/C$	14: 57: 29	7: 61: 32
$Pt_1Pd_3Cu_3/C$	14: 43: 43	9: 42: 49

Table 5. The stoichiometric, real atomic ratios and real metallic loadings analyzed from ICP-OES in the $Pt_1Pd_1Cu_1/C$, $Pt_1Pd_2Cu_1/C$, $Pt_1Pd_5Cu_1/C$, $Pt_1Pd_4Cu_2/C$, $Pt_1Pd_3Cu_3/C$ catalysts

Sample	Stoichiometric atomic ratio of Pt to Pd to Cu	Atomic ratio of Pt to Pd to Cu from ICP-OES	Metallic loading (wt %)
$Pt_1Pd_1Cu_1/C$	33: 33: 33	35: 35: 30	16.9
$Pt_1Pd_2Cu_1/C$	25: 50: 25	28: 52: 20	17.7
$Pt_1Pd_5Cu_1/C$	14: 72: 14	16: 72: 12	19.0
$Pt_1Pd_4Cu_2/C$	14: 57: 29	15: 61: 24	18.8
$Pt_1Pd_3Cu_3/C$	14: 43: 43	17: 50: 33	20.0

3.2. Electrochemical characterization

Figure 6 shows the cyclic voltammograms of the $Pt_1Pd_1Cu_1/C$, $Pt_1Pd_2Cu_1/C$, $Pt_1Pd_5Cu_1/C$, $Pt_1Pd_4Cu_2/C$, $Pt_1Pd_3Cu_3/C$ catalysts in N_2-saturated $HClO_4$ solution. The typical CV characteristics of a "platinum-like" or "palladium-like" catalyst, as revealed by the obvious hydrogen desorption/adsorption current peaks at low potential range (i. e., -0.2-0.1 V) and surface oxidation/reduction at high potential range (i. e., higher than 0.3 V) can be observed on all the Pt-Pd-

Cu/C catalysts. Besides, the Pt-Pd-Cu/C catalysts with different compositions exhibit similar mass-normalized surface oxidation/reduction currents, indicating similar electrochemical surface areas of the five catalysts.
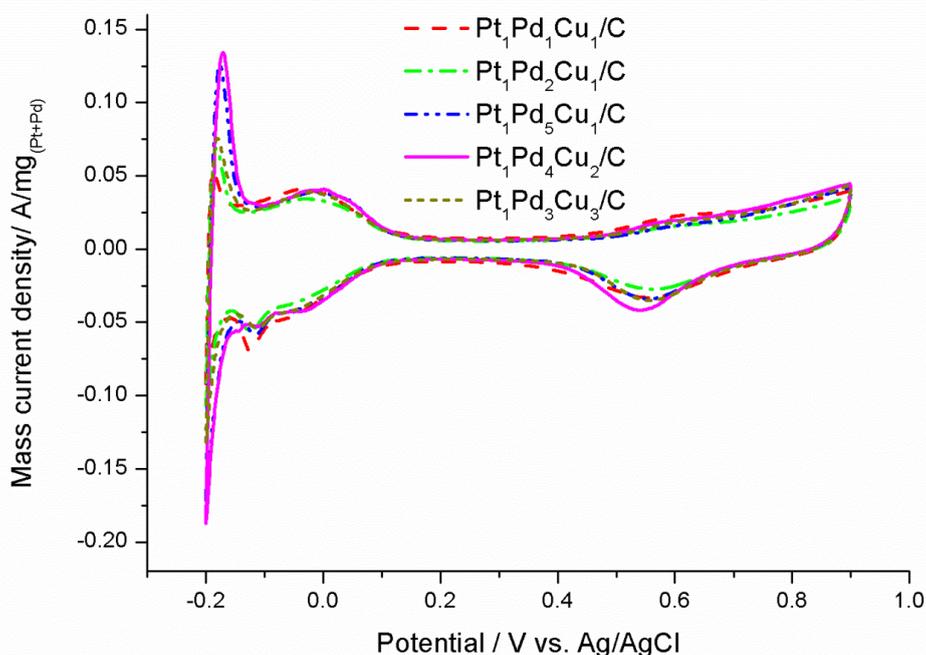
Figure 6. Cyclic voltammograms of the $Pt_1Pd_1Cu_1/C$, $Pt_1Pd_2Cu_1/C$, $Pt_1Pd_5Cu_1/C$, $Pt_1Pd_4Cu_2/C$, $Pt_1Pd_3Cu_3/C$ catalysts in N_2-saturated 0.5 M $HClO_4$ solution at 25 ^{o}C with scan rate of 50 mV/s

Figure 7 shows the polarization curves of formic acid oxidation on Pt/C, Pd/C, $Pt_1Pd_1Cu_1/C$, $Pt_1Pd_2Cu_1/C$, $Pt_1Pd_5Cu_1/C$, $Pt_1Pd_4Cu_2/C$, $Pt_1Pd_3Cu_3/C$ catalysts. The currents were normalized to the total mass of Pt and Pd on the glassy carbon electrode to give mass current densities. Typical CV feature of formic acid oxidation on Pt, with two anodic peaks in the forward scan and one anodic peak in the backward scan can be observed on the Pt/C catalyst. The mechanism of formic acid oxidation on Pt has been widely studied and it is now accepted that formic acid oxidation on Pt follows a dual-path mechanism, which involves a dehydrogenation pathway to form CO_2 directly and a dehydration pathway with the formation of adsorbed intermediate species (CO_{ads}). The adsorbed CO species could occupy the active surface of Pt and thus inhibit formic oxidation reaction on Pt. The CO_{ads} can be removed by the aid of adsorbed OH_{ads} species formed at high potential range. In the forward scan, the first oxidation peak at low potential range (i. e., lower than 0.4 V) corresponds to the direct oxidation of formic acid on the unblocked Pt surface and the second oxidation peak at high potential range (i. e., higher than 0.6 V) is related to the oxidation of CO_{ads}. Removal of the CO_{ads} releasing fresh Pt surface, results in the large oxidation peak in the backward scan. The peak current densities of the first and second oxidation peaks in the forward scan are denoted as I_{pa}^{d} and I_{pa}^{ind} respectively. The peak current density of formic acid oxidation in the backward scan is denoted as I_{pc}.
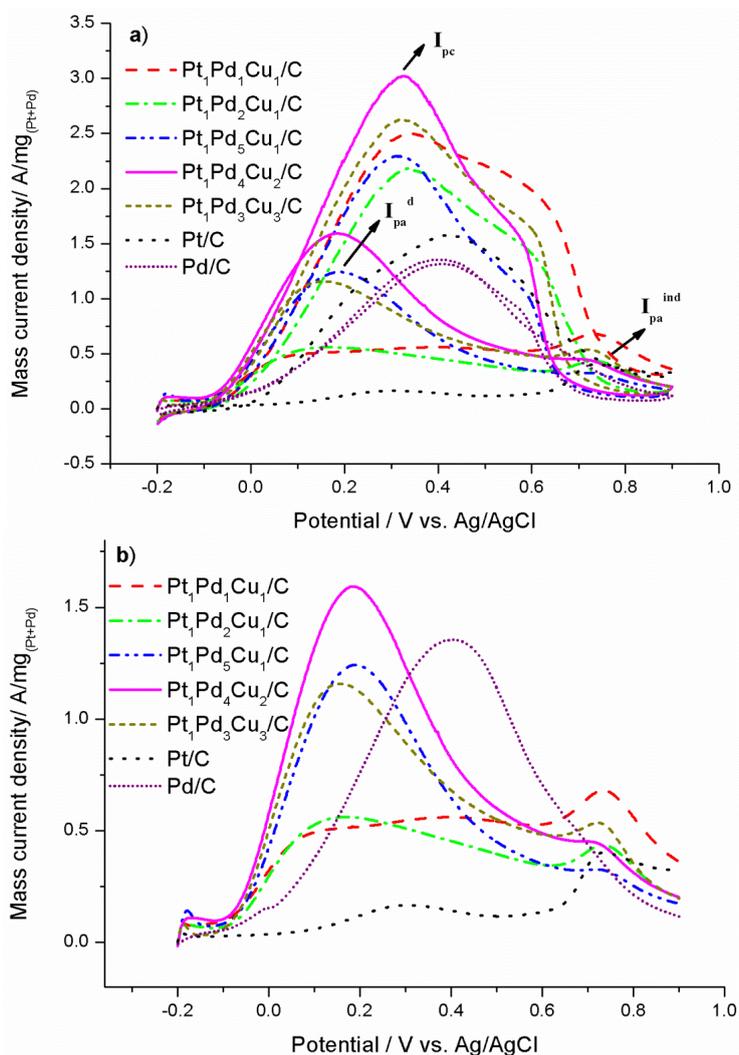
Figure 7. a) Cyclic voltammograms of the $Pt_1Pd_1Cu_1/C$, $Pt_1Pd_2Cu_1/C$, $Pt_1Pd_5Cu_1/C$, $Pt_1Pd_4Cu_2/C$, $Pt_1Pd_3Cu_3/C$ catalysts in N_2-saturated 0.5 M HCOOH + 0.5 M $HClO_4$ at 25 ^{o}C with scan rate of 50 mV/s; **b)** The forward scan (Figure 7a) of formic acid oxidation on the different catalysts

Table 6 shows the values of I_{pa}^d, I_{pa}^{ind} and I_{pc} on all the catalysts containing Pt. It can be seen that both the peak current densities of the first oxidation peak in the forward scan (I_{pa}^d) and the peak current densities in the backward scan (I_{pc}) on all the five Pt-Pd-Cu/C catalysts are much higher than that on Pt/C. Especially, $Pt_1Pd_4Cu_2/C$ exhibits the highest mass current density, with I_{pa}^d of 1.59, which is about 9.4 times that of Pt/C. The ratio of I_{pa}^d to I_{pa}^{ind} is considered to be the indication for which pathway is dominant [31]. From Table 6, it can be seen that the ratios of I_{pa}^d to I_{pa}^{ind} on the all the Pt-Pd-Cu/C catalysts are larger than that on Pt/C. Especially, the ratio of I_{pa}^d to I_{pa}^{ind} on $Pt_1Pd_5Cu_1/C$, $Pt_1Pd_4Cu_2/C$ are larger than 3, suggesting formic acid oxidation mainly follows the dehydrogenation pathway with much less CO_{ads} formation on these two catalysts. It is now accepted that the dehydration of formic acid to form CO_{ads} requires at least more than one adjacent Pt atoms [32-34]. The incorporation of Pd and Cu to Pt could result in the arrangement of Pd or Cu around Pt. These "isolated" Pt could favor the direct oxidation of formic acid. The catalytic activity of Pd/C for formic acid oxidation was also evaluated for comparison, as shown in Figure 7b. It can be seen that, in terms

of the forward scan, the potentials of the first oxidation peak on $Pt_1Pd_5Cu_1/C$, $Pt_1Pd_4Cu_2/C$, $Pt_1Pd_3Cu_3/C$ catalysts are much lower than that on Pd/C. The oxidation current densities on the five Pt-Pd-Cu/C catalysts in the backward scan are all much larger than that on Pd/C (as shown in Figure 7a), suggesting high activities of the Pt-Pd-Cu/C catalysts compared with Pd/C. Moreover, the mass normalized peak current density on our $Pt_1Pd_4Cu_2/C$ catalyst in the backward scan (i. e., 3.02 $A/mg_{(Pt+Pd)}$) is higher than the previous reports, such as 0.186 $A/mg_{(Pt)}$ on $Pt_{79}Fe_{21}$/nitrogen-doped graphene catalyst (0.5 M H_2SO_4 + 1 M HCOOH, scan rate of 50 mV/s) [8], about 0.81 $A/mg_{(Pt)}$ on $Pt_{10}Au_{10}Cu_{80}/C$ catalyst (0.5 M H_2SO_4 + 0.5 M HCOOH, scan rate of 50 mV/s) [35], about 0.63 $A/mg_{(Pt+Pd)}$ on PtPd/CNTs catalyst (0.5 M H_2SO_4 + 0.5 M HCOOH, scan rate of 50 mV/s) [36], about 1.1 $A/mg_{(Pt+Pd)}$ on $Pt_{0.5}Pd_{0.5}/C$ catalyst (0.1 M H_2SO_4 + 0.1 M HCOOH, scan rate of 10 mV/s) [37], 2.471 A/ $mg_{(Pd)}$ on PdNi/C (0.1 M $HClO_4$ + 0.5 M HCOOH, scan rate of 50 mV/s) [38]. Our results demonstrate the importance of Pt-Pd-Cu/C trimetallic material as formic acid oxidation catalyst.

Table 6. The peak current densities of the first formic acid oxidaiton peak (I_p^d), the second formic acid oxidation peak (I_p^{ind}) in the forward scan and the peak current densities in the backward scan (I_p^b) on the Pt/C, $Pt_1Pd_1Cu_1/C$, $Pt_1Pd_2Cu_1/C$, $Pt_1Pd_5Cu_1/C$, $Pt_1Pd_4Cu_2/C$, $Pt_1Pd_3Cu_3/C$ catalysts

Sample	I_{pa}^d ($A/mg_{(Pt+Pd)}$)	I_{pa}^{ind} ($A/mg_{(Pt+Pd)}$)	I_{pc} ($A/mg_{(Pt+Pd)}$)	I_{pa}^d/ I_{pa}^{ind}
Pt/C	0.17	0.40	1.58	0.43
$Pt_1Pd_1Cu_1/C$	0.50	0.68	2.50	0.74
$Pt_1Pd_2Cu_1/C$	0.56	0.44	2.18	1.27
$Pt_1Pd_5Cu_1/C$	1.24	0.33	2.29	3.76
$Pt_1Pd_4Cu_2/C$	1.59	0.45	3.02	3.53
$Pt_1Pd_3Cu_3/C$	1.16	0.54	2.63	2.15

4. CONCLUSIONS

In this work, a series of carbon supported Pt-Pd-Cu trimetallic (Pt-Pd-Cu/C) nano-catalysts were prepared towards formic acid oxidation reaction. The catalysts were synthesized through simply co-reduction of Pt, Pd and Cu ions using ethylene glycol and sodium citrate as the reducing and stabilizing reagents. XRD characterization suggests that Pt-Pd-Cu alloys with different lattice parameters can be successfully prepared through adjusting the atomic ratios of Pt, Pd and Cu ions in the precursor solutions. The average crystal sizes of the Pt-Cu/C catalysts are in the range of 2.7-3.1 nm. Electrochemical analysis suggests that Pt-Pd-Cu/C catalysts exhibit high mass activities towards formic acid oxidation reaction and the activities are dependent on the composition of the catalysts, with $Pt_1Pd_4Cu_2/C$ exhibiting the highest value.

References

1. J. Jiang and A. Kucernak, *J. Electroanal. Chem.*, 520 (2002) 64.
2. Z. Liu, L. Hong, M. Tham, T. Lim and H. Jiang, *J. Power Sources*, 161 (2006) 831.
3. A. Capon and R. Parsons, *J. Electroanal. Chem.*, 44 (1973) 1.
4. J. Lović, A. Tripković, S. Gojković, K. Popović, D. Tripković, P. Olszewski and A. Kowal, *J. Electroanal. Chem.,* 581 (2005) 294.
5. M. Arenz, V. Stamenkovia, T. Schmidt, K. Wandelt, P. Ross and N. Markovia, *Phys. Chem. Chem. Phys.*, 5 (2003) 4242.
6. W. Jung, J. Han, S. Yoon, S. Nam, T. Lim and S. Hong, *J. Power Sources*, 196 (2011) 4573.
7. Y. Qin, X. Zhang, X. Dai, H. Sun, Y. Yang, X. Li, Q. Shi, D. Gao, H. Wang, N. Yu and S. Sun, *Small*, 12 (2016) 524.
8. Y. Sun, T. Zhou, Q. Pan, X. Zhang and J. Guo, *RSC Advances,* 5 (2015) 60237.
9. B. Zhang, C. He, Y. Jiang, M. Chen, Y. Li, L. Rao, and S. Sun, *Electrochem. Commun.*, 25 (2012) 105.
10. J. Xu, T. Zhao, Z. Liang and L. Zhu, *J. Phys. Chem. C*, 112 (2008) 17362.
11. B. Habibi and N. Delnavaz, *RSC Advances*, 2 (2012) 1609.
12. H. Qiu, H. Xu, X. Li, J. Wang and Y. Wang, *J. Mater. Chem. A*, 3 (2015) 7939.
13. J. Chen, Y. Li, S. Liu, G. Wang, J. Tian, C. Jiang, S. Zhu and R. Wang, *Appl. Surf. Sci.*, 287 (2013) 457.
14. X. Wang and Y. Xia, *Electrochem. Commun.*, 10 (2008) 1644.
15. K. Ding, L. Liu, Y. Cao, X. Yan and H. Wei, *Int. J. Hydrogen Energy*, 39 (2014) 7326.
16. Z. Bai, L. Yang, J. Zhang, L. Li, J. Lv, C. Hu and J. Zhou, *Catal. Commun.* 11 (2010) 919.
17. Y. Lu and W. Chen, *ACS Catalysis*, 2 (2012) 84.
18. W. Wen, C. Li, W. Li and Y. Tian, *Electrochim. Acta*, 109 (2013) 201.
19. Y. Fan, Y. Zhang, H. Li, W. Shen, J. Wang and M. Wei, *RSC Advances*, 6 (2016) 43980.
20. S. Lee, N. Jung, J. Cho, H. Park, J. Ryu, I. Jang, H. Kim, E. Cho, Y. Park, H. Ham, J. Jang and S. Yoo, *ACS Catalysis*, 4 (2014) 2402.
21. J. Lee, D. Kwak, Y. Lee, S. Lee and K. Park, *Phys. Chem. Chem. Phys.*, 17 (2015) 8624.
22. S. Hu, L. Scudiero and S. Ha, *Electrochim. Acta*, 83 (2012) 354.
23. J. Chen, Y. Li, Z. Gao, G. Wang, J. Tian, C. Jiang, S. Zhu and R. Wang, *Electrochem. Commun.*, 37 (2013) 24.
24. S. Li, D. Cheng, X. Qiu and D. Cao, *Electrochim. Acta*, 143 (2014) 44.
25. B. Yu, W. Wen, W. Li, Y. Yang, D. Hou and C. Liu, *Electrochim. Acta*, 196 (2016) 223.
26. G. Fu, B. Xia, R. Ma, Y. Chen, Y. Tang and J. Lee, *Nano Energy*, 12 (2015) 824.
27. C. Cui, H. Li, H. Cong, S. Yu and F. Tao, *Chem. Commun.*, 48 (2012) 12062.
28. K. Jiang and W. Cai, *Appl. Catal. B-Environ.*, 147 (2014) 185.
29. Y. Suo and I. Hsing, *Electrochim. Acta*, 56 (2011) 2174.
30. R. Jenkins and R. Snyder, *Introduction to X-ray powder diffractometry*, John Wiley & Sons, Inc., (1996) New York , USA.
31. M. Xiao, S. Li, J. Zhu, K. Li, C. Liu and W. Xing, *ChemPlusChem*, 79 (2014) 1123.
32. H. Zhang, C. Wang, J. Wang, J. Zhai and W. Cai, *J. Phys. Chem. C*, 114 (2010) 6446.

33. M. Neurock, M. Janik and A. Wieckowski, *Faraday Discuss.*, 140 (2008) 363.
34. B. Gralec and A. Lewera, *Appl. Catal. B-Environ.*, 192 (2016) 304.
35. M. Wang, Y. He, R. Li, Z. Ma, Z. Zhang and X. Wang, *Electrochim. Acta*, 178 (2015) 259.
36. B. Liu, H. Li, L. Die, X. Zhang, Z. Fan and J. Chen. *J. Power Sources*, 186 (2009) 62.
37. E. Baranova, N. Miles, P. Mercier, Y. Page and B. Patarachao, *Electrochim. Acta*, 55 (2010) 8182.
38. M. Matin, J. Jang and Y. Kwon, *J Power Sources*, 262 (2014) 356.